Advanced Imaging in Glioma Treatment

Verburg, N.

2020

Niels Verburg
Floris P. Barthel
Kevin J. Anderson
Kevin C. Johnson
Thomas Koopman
Maqsood M. Yaqub
Otto S. Hoekstra
Adriaan A. Lammertsma
Frederik Barkhof
Jeroen A.M. Belien
Petra J.W. Pouwels
Jaap C. Reijneveld
Jan J. Heimans
Annemieke J.M. Rozemuller
Ronald Boellaard
Michael D. Taylor
Joseph F. Costello
W. Peter Vandertop
Pieter Wesseling
Philip C. de Witt Hamer
Roel G.W. Verhaak

In preparation

Chapter 10

The DNA methylation landscape of core and peripheral regions in diffuse glioma shows little spatial heterogeneity after considering tumor purity

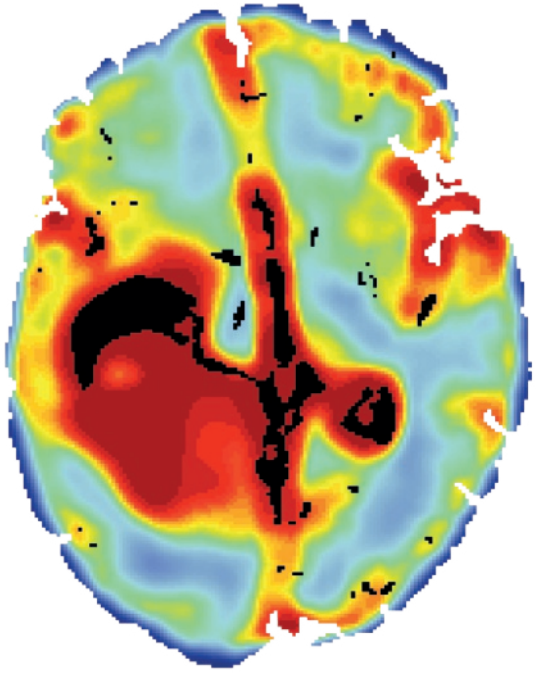

ABSTRACT

Diffuse gliomas are notorious for their histopathological, genetic and transcriptional spatial heterogeneity. Little is known about the DNA methylation spatial heterogeneity in glioma. Genomic analysis of tumors is strongly influenced by tumor purity. Using image-guided multi-sector stereotactic biopsy samples acquired in core and peripheral regions, DNA methylation profiles and histological, radiological and molecular measurement modalities of tumor purity were analyzed and compared. We show that DNA methylation-derived assessment of tumor purity is the most representative for all these measurement modalities. Using this tumor purity metric, we demonstrate that tumor purity is highly variable between samples within patients. Apparent spatial heterogeneity in DNA methylation classification can be explained by variation in tumor purity and generally does not reflect biological variation. Genome-wide DNA methylation analysis at individual probe level confirms intratumoral methylation stability. These findings underline the importance of tumor purity measurement for optimal interpretation of the results of DNA methylation assessment of intratumoral heterogeneity as well as the robustness of characterization of diffuse gliomas based on DNA methylation patterns.

INTRODUCTION

Diffuse gliomas are the most common primary brain tumors in adults and have a poor prognosis despite multimodal treatment.[1] This therapy resistance is, among others, contributed to the spatial heterogeneity that has been demonstrated in histopathological, genetic and transcriptional studies.[327,332-334] At the genomic level, copy number alteration (CNA) heterogeneity is reflected by CNAs that are shared between specimens obtained from different regions from the same tumor, coexisting with CNAs unique to one area of the tumor.[334] A similar pattern of CNA heterogeneity can be found at the single-cell level.[335] Besides CNAs, both spatial and temporal heterogeneity in driver gene mutations can also be observed [333] At the transcription level, spatial heterogeneity of molecular subtypes has been reported at both sample and single-cell level.[327,334]

Much less is known about epigenetic heterogeneity in diffuse gliomas and its potential impact on therapy resistance. Where genetic heterogeneity is driven by clonal evolution,[336] epigenetic heterogeneity could be driven by clonal evolution, microenvironmental factors, differentiation from cancer stem cells or a combination thereof.[337] In glioma, the evolutionary history of DNA methylation changes and somatic mutations were comparable, with most mutation and methylation changes occurring in different sets of genes.[338] DNA methylation heterogeneity did not typically occur in known tumor driver genes,[338] but mostly in open sea regions.[339] Together with the findings that promoter site DNA methylation heterogeneity and expression of target genes does not correlate well, this could imply that DNA methylation changes in tumors that alter gene expression are relatively stable.[340] Indeed, epigenetic molecular subtypes of diffuse glioma have been described, suggesting that commonalities in epigenetic glioma profiles exist.[341] However, a recent study reported spatial heterogeneity of epigenetic molecular subtypes in glioblastoma,[339] using the epigenetic molecular subtypes of Capper et al.[342] Interestingly, patients with epigenetic molecular subtype heterogeneity displayed lower overall tumor purity and higher variance in tumor purity than patients without epigenetic molecular subtype heterogeneity. This indicates that tumor purity could have influenced these results. Of note, this study focused on samples from regions with contrast enhancement on magnetic resonance imaging (MRI), and did not include DNA methylation profiling of regions without contrast enhancement but with glioma infiltration.[3,4] Non-enhancing regions are of great interest, since they are not typically resected during surgery and then a source of residual glioma cells.

In order to improve our understanding of epigenetic spatial heterogeneity of diffuse gliomas, we present the DNA methylation landscape of core and peripheral samples of such tumors focusing on molecular subtypes and genome-wide methylation while taking tumor purity into account. Validation is provided by two cohorts; one with initial glioma multi-sector core samples and the other with non-glioma brain samples.

RESULTS

We analyzed 133 multi-region image-guided stereotactic samples from 16 newly diagnosed and untreated patients with a diffuse glioma, obtained preceding craniotomy for the first surgical resection (Figure 1). Samples in this exploration cohort were derived from: diffuse astrocytoma, IDH-mutant (n=6); oligodendroglioma, IDH-mutant and 1p19q-codeleted (n=1); glioblastoma, IDH-wildtype (n=7); glioblastoma, IDH-mutant (n=2). DNA methylomes were profiled using the Illumina 850k EPIC bead array. Histopathological hematoxylin-and-eosin (H&E) and MIB-1 images were digitized, distance to tumor-surface was calculated and T1-weighted contrast-enhanced (T1c) and FLAIR MRI abnormalities at sample location were scored.

We constructed a second cohort consisting of 61 multi-region DNA methylomes from 11 adult patients with a glioma, including diffuse astrocytoma, IDH-mutant (n=2); oligodendroglioma and 1p19q-codeleted, IDH-mutant (n=3); anaplastic oligodendroglioma, IDH-mutant and 1p19q-codeleted (n=1); anaplastic astrocytoma, IDH-mutant (n=1); glioblastoma, IDH-wildtype (n=4).[338,343] For comparison, we also obtained a set of DNA methylation profiles from 64 non-neoplastic brain samples.[342]

Tumor purity is most representatively estimated by a DNA methylation-derived metric

Since non-neoplastic cells in a sample influence molecular tumor classification,[344] it is necessary to determine the tumor purity of samples in order to quantify the ratio neoplastic/non-neoplastic cells. To establish the most representative tumor purity metric, we set out to compare for each tumor sample seven purity metrics: 1). Tumor cellularity, defined as median number of cells per mm^2, derived by computational analysis of the complete histological slide; 2) proliferation index, defined as median percentage of MIB-1-positive cells, derived by computational analysis of the complete slide; 3) distance-to-tumor-surface (DTTS), defined as the Euclidean distance between the sample location and abnormalities on T1c MRI for enhancing gliomas and on FLAIR MRI for non-enhancing gliomas; 4) imaging score, which was based on the qualitative

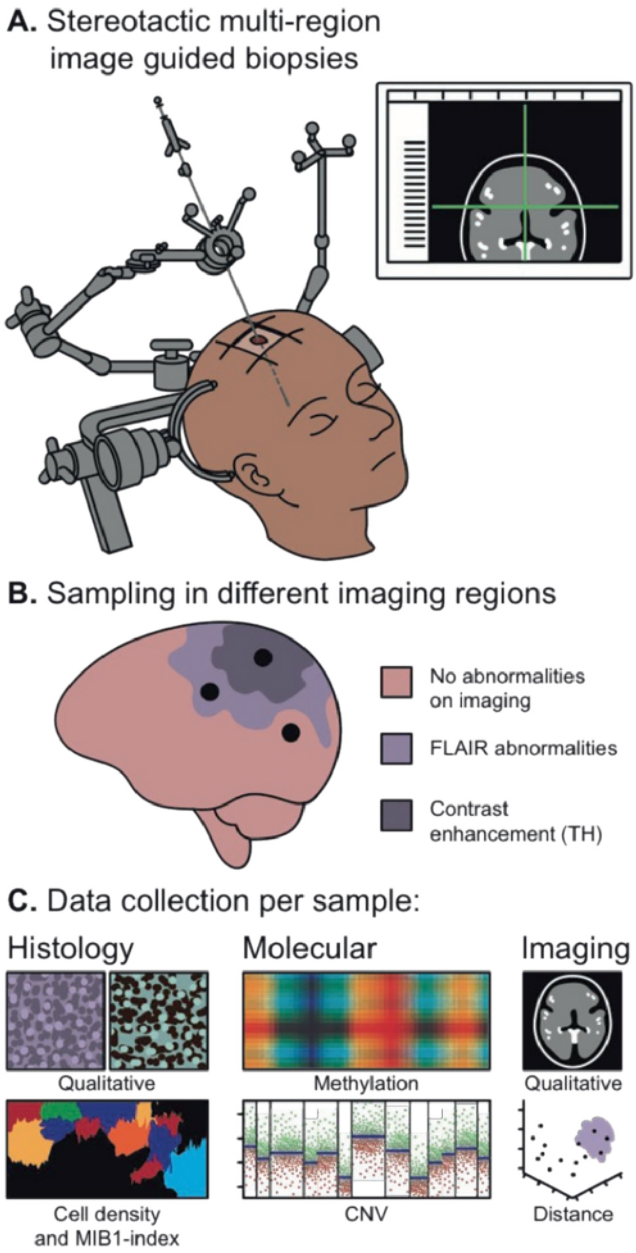

Figure 1 | Graphical overview of methods.

assessment of imaging abnormalities of standard MRI sequences at the sample location; 5) purity assessment from clonal methylation sites (PAMES);[345] 6) simplicity score of methylation classification as defined by Wang et al.;[344] and 7) aneuploidy score, based on

methylation-derived copy-number variation (CNV). An overview of all modalities in the exploration cohort is given in Figure 2. The distributions of the individual measurement modalities are presented in Supplementary Figure 1.

The correlation between the measurement modalities varied, with PAMES most correlated with all other modalities (Figure 3A and 3B), therefore used as most representative tumor purity metric for further analyses. PAMES correlated best with simplicity score, both methylation-derived measurements although based on different probes,[344,345] and least with the proliferation index, in line with previous reports.[346,347] As expected, modalities correlated best with modalities from the same field, i.e. histology, radiology and DNA methylation. DTTS was not correlated with proliferation in all samples (Suppl. Figure 2A) and samples from IDH-mutant gliomas (Supplementary Figure 2B). However, there was a weak, yet significant, negative correlation (r=-0.28, p=0.023) in samples from IDH-wildtype gliomas (Supplementary Figure 2B). The absence of a correlation in IDH-mutant gliomas is most likely due to the low overall proliferation index (supplementary Figure 2C).

Median tumor purity was 60.5% [IQR 30.4%] compared to 84.9% [IQR 4.4%] in the validation cohort. The higher tumor purity in the validation cohort may partly be explained by the lack of peripheral samples in this cohort. Median tumor purity in the core samples of the exploration cohort was 73.6% [IQR 17.9%]. Tumor purity was higher in samples from IDH-mutant than from IDH-wildtype gliomas and higher in samples from low-grade than high-grade gliomas (Figure 3C). This latter finding is concordant with previous studies[346,347] and might be explained by a higher percentage of non-neoplastic (e.g. stromal and/or immune) cells in high-grade gliomas.[347] In the validation cohort, however, no difference was found in tumor purity according to IDH mutational status.

Assessment of tumor presence by neuropathologists differs from epigenetic classification

In daily clinical practice, glioma tissue from stereotactic biopsies or surgical resection is assessed by neuropathologist for, among others, tumor presence, using histological slides, all or not including immune-histochemical stainings. DNA methylation profiling is gaining interest as a diagnostic tool for the neuropathologist.[342] To establish the correlation between tumor presence/absence as assessed on histology and epigenetic molecular subtypes, we compared the consensus assessment of tumor presence by two neuropathologists with molecular subtypes. Since our image-guided cohort was expected to contain non-tumor samples as well, we used a machine learning approach with the

TCGA training data and the samples from our non-glioma cohort to extend the seven epigenetic molecular subtypes from Ceccarelli et al. (G-CIMP-low, G-CIMP-high, Codel, Classical, Mesenchymal, PA-like, LGm6) with three subtypes: Cortex, Inflammatory and Reactive.[341] All samples with the subtypes Classical (n=18), Mesenchymal (n=9) and Codel (n=5) were assessed as containing tumor by the neuropathologists (Figure 4A). Of the 39 G-CIMP-high samples, all but one were assessed as containing tumor as well. All samples classified with the subtypes Inflammatory (n=3) and Reactive (n=1) were assessed as tumor. This was confirmed by the tumor purity and DTTS of these samples, which was comparable to those of epigenetic molecular tumor subtypes and significantly different from the Cortex subtype (Figure 4B). Therefore all epigenetic molecular subtypes except for Cortex were considered as evidence of tumor presence. Of the 58 samples classified as Cortex, 34 were assessed as normal and 24 as tumor. Other way around, 1 of the 35 samples assessed as normal (3%) was classified as G-CIMP-high, while 24 of the 98 samples assessed as tumor were classified as Cortex (24%) (Figure 4C). These findings show a considerable discordance between tumor presence assessed by histopathology and epigenetic molecular subtype classification. To identify the underlying causes of the discordance, we explored tumor purity and simplicity score, which influence molecular subtyping, as well as cellularity and proliferation index, which are used for the histological assessment. In the single G-CIMP-high sample assessed as normal, tumor purity was 60% and simplicity score 99%, both confirming the epigenetic molecular subtype classification as tumor.

Cellularity and proliferation index, however, were 1585 cells/mm2 and 0.38%, which was considerable lower than the mean cellularity and proliferation index in the epigenetic molecular subtypes indicative of tumor presence (2690 cells/mm^2 and 2.1%, respectively) (Figure 4D). In samples assessed as tumor, higher tumor purity and simplicity scores were found for samples with an epigenetic molecular subtype indicative of tumor presence (n=74) compared with Cortex subtype samples (n=24) (both $p<0.01$). Interestingly, cellularity was also higher in samples with an epigenetic molecular subtypes indicative of tumor presence compared to Cortex subtype samples ($p<0.01$) (Figure 4D). This implies that the neuropathologists did not always use cellularity as indicator of tumor presence and may have used other histological features (e.g. proliferation index based on Ki-67 immunohistochemistry or nuclear pleiomorphism) as well. Although proliferation index is an established marker for tumor presence,[28] it can also be increased due to inflammation and presence of microglial cells.[348] This could be an explanation for the discordance between the neuropathologists and molecular subtypes. An alternative explanation is an underestimation of tumor presence by DNA methylation.

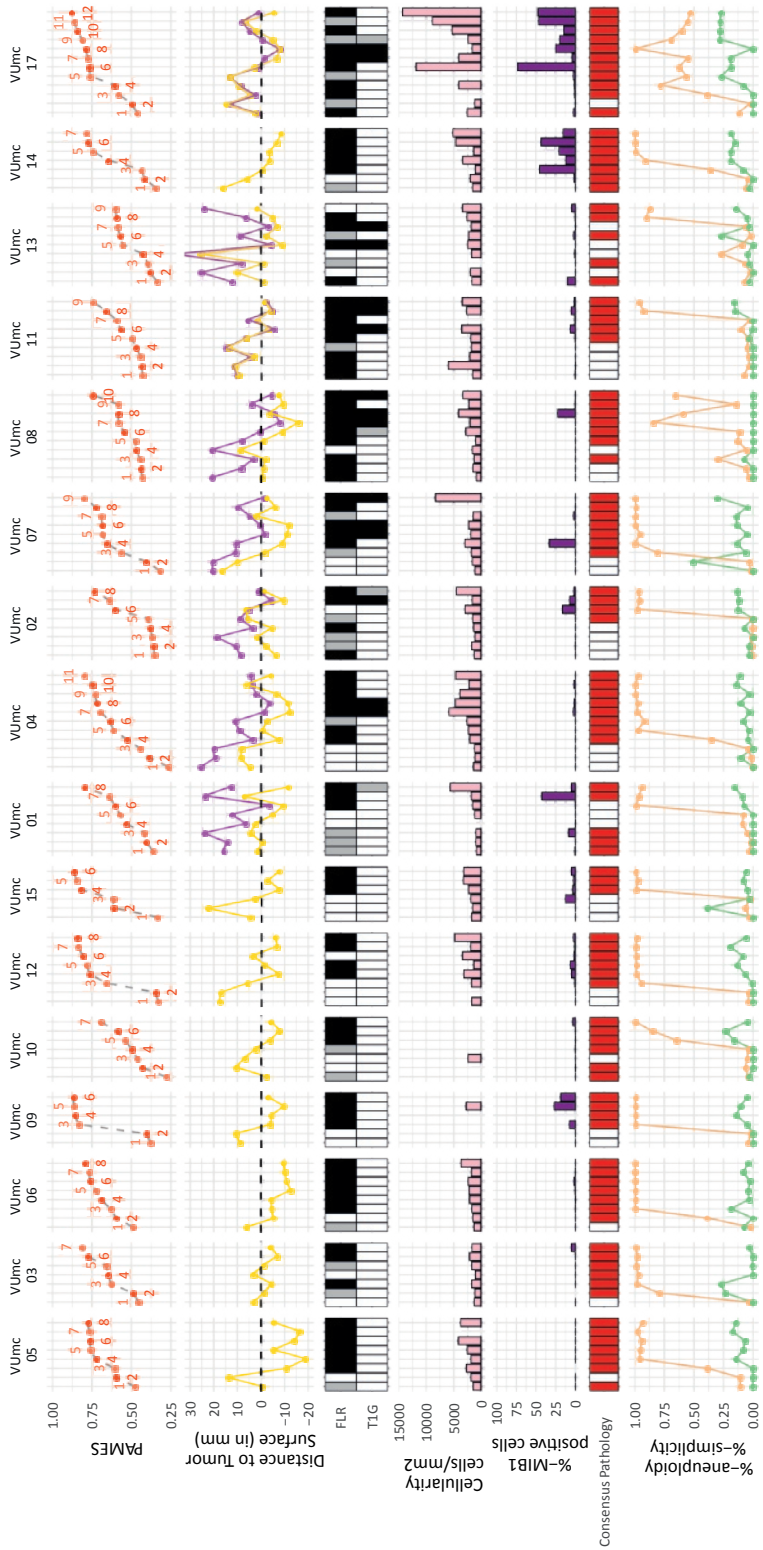

Figure 2 | Overview of 133 samples in 16 patients with primary diffuse glioma.

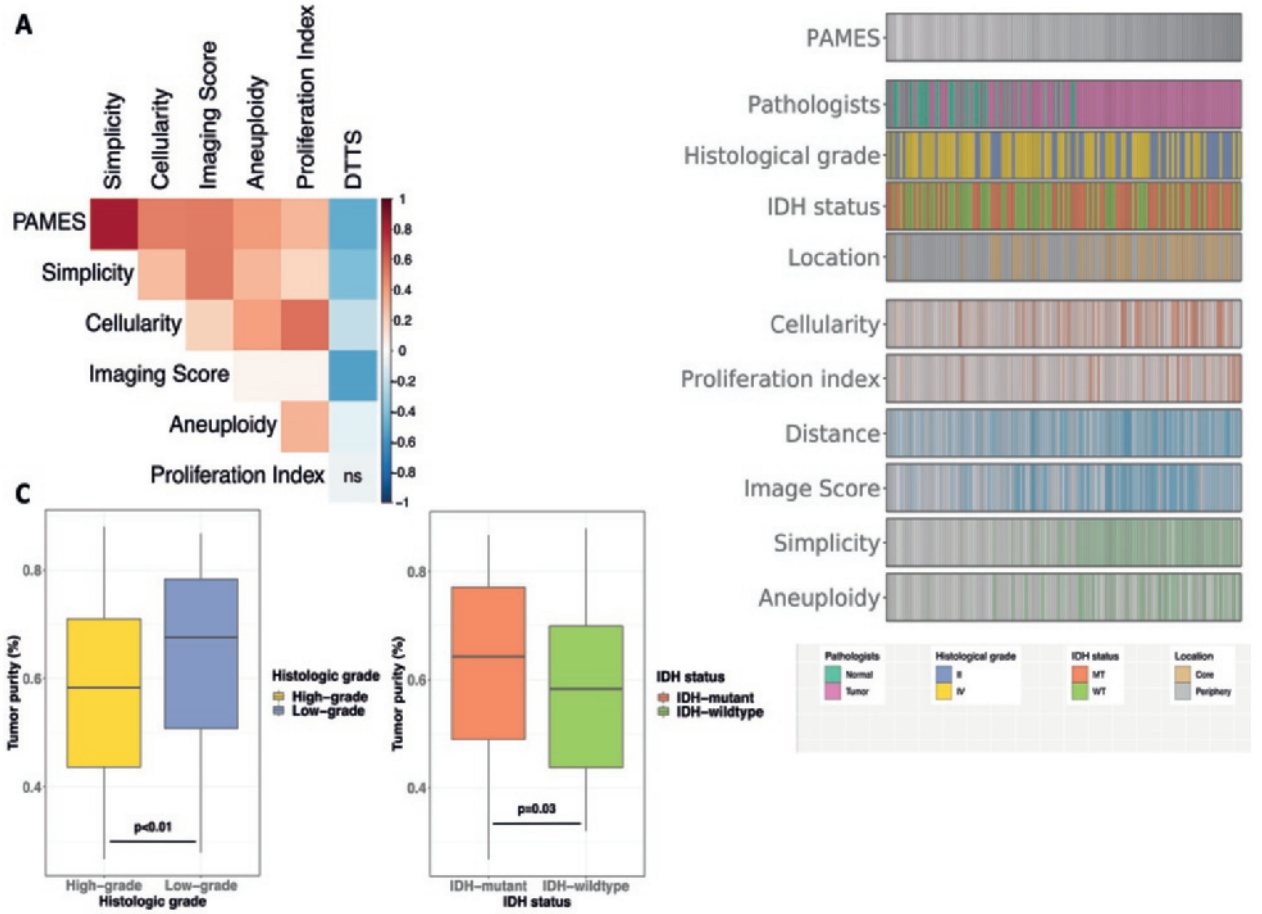

Figure 3 | Purity measurment modalitites. A) Correlation plot of modalititiees wit spearman correlation represented as color, ns =non-significant. B) Landscape of purity measurment modalities ordered from low tohigh purity using PAMES. C) Boxplots of tumor purity for histological grade (*left*) and IDH mutational status (*right*).

Spatial distribution differs between IDH-mutant and IDH-wildtype gliomas

To understand the spatial distribution of glioma infiltration, we explored the correlation of tumor purity, epigenetic molecular subtypes and neuropathological assessment with MRI abnormalities. First, tumor purity of regions with and without imaging abnormalities was compared. As expected, regions with imaging abnormalities demonstrated a higher tumor purity than regions without imaging abnormalities ($p<0.01$) (Figure 5A). This was true for both IDH-mutant and IDH-wildtype gliomas (Figure 5B), although the difference in tumor purity between abnormal and normal regions was considerably larger in IDH-mutant gliomas (26.9%) than in IDH-wildtype gliomas (16.1%). Since MRI abnormalities were based on both T1c and FLAIR, we examined the tumor purity of these different regions (Figure 5C). In IDH-mutant gliomas, regions with FLAIR but without T1c abnormalities (T1c- FLAIR+) showed a higher tumor purity than regions without MRI abnormalities (T1c- FLAIR-) ($p<0.01$). Interestingly, this was not the case in IDH-wildtype gliomas. Comparing the FLAIR+T1c- regions with the regions with both FLAIR and T1c abnormalities (T1c+ FLAIR+) demonstrated a higher tumor purity in the FLAIR+T1c+ regions in IDH-wildtype gliomas ($p<0.01$), yet not in IDH-mutant gliomas.

These findings imply that IDH-mutant and IDH-wildtype gliomas have different growth patterns. IDH-mutant gliomas are more compact considering the large difference between the T1c-FLAIR- and both T1c-FLAIR+ and T1c+FLAIR + regions, as well as the similarity between the T1c-FLAIR+ and T1c+FLAIR + regions. IDH-wildtype gliomas are more diffuse, since there is no difference between the T1c-FLAIR- and T1c-FLAIR+ regions and there is a difference between the T1c-FLAIR+ and T1c+FLAIR+ region. An alternative explanation would be that, in contrast to IDH-mutant gliomas, the T1c-FLAIR+ region in IDH-wildtype gliomas does not necessarily contain tumor. Therefore we explored the epigenetic molecular subtypes (Figure 5D) and neuropathologist's assessment (Figure 5E) for the different regions. Since 38% of the samples had an epigenetic molecular subtype and 28% were assessed as tumor, it can be concluded that the T1c-FLAIR+ region in IDH-wildtype gliomas also contains tumor. Interestingly, although the difference was not significant, the T1c-FLAIR- region in IDH-wildtype gliomas showed epigenetic molecular tumor subtypes in 25% and assessment as tumor in 38% of samples, compared to respectively 15% and 25% in IDH-mutant gliomas. When comparing the number of patients with epigenetic tumor subtypes in more than one MRI region we found a higher percentage for IDH-wildtype (86%) than IDH-mutant gliomas (44%) (Figure 5F). This difference, however, was not significant (Fisher's test $p=0.15$), most likely due to the limited number of patients. These findings support the concept

that IDH-wildtype gliomas show more extensive diffuse infiltrative growth at the time of first surgical intervention than IDH-mutant gliomas.

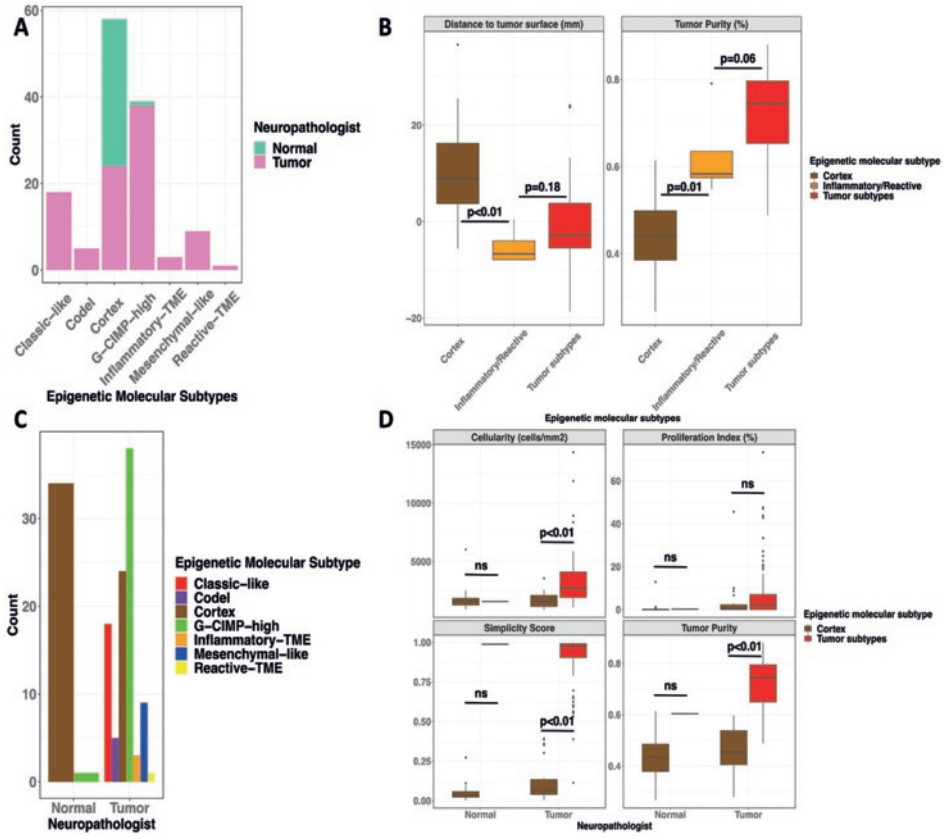

Figure 4 | Assessment of tumor presence by neuropathologists and DNA methylation.

A) Bar plot of epigenetic molecular subtypes for samples assessed as normal and tumor. B) Boxplot of DTTS (*left*) and tumor purity (*right*) for the epigenetic molecular subtypes 1) Cortex, 2) Inflammatory and Reactive and 3) Tumor subtypes (Codel, G-CIMP-high, Classic and Mesenchymal). C) Bar plot of epigenetic molecular subtypes of samples assessed as normal or tumor by the neuropathologist. D) Box plots of cellularity (*left upper*), proliferation index (*right upper*), simplicity score (*left bottom*) and tumor purity (*right bottom*) for samples assessed as normal or tumor and with an epigenetic tumor or Cortex subtype.

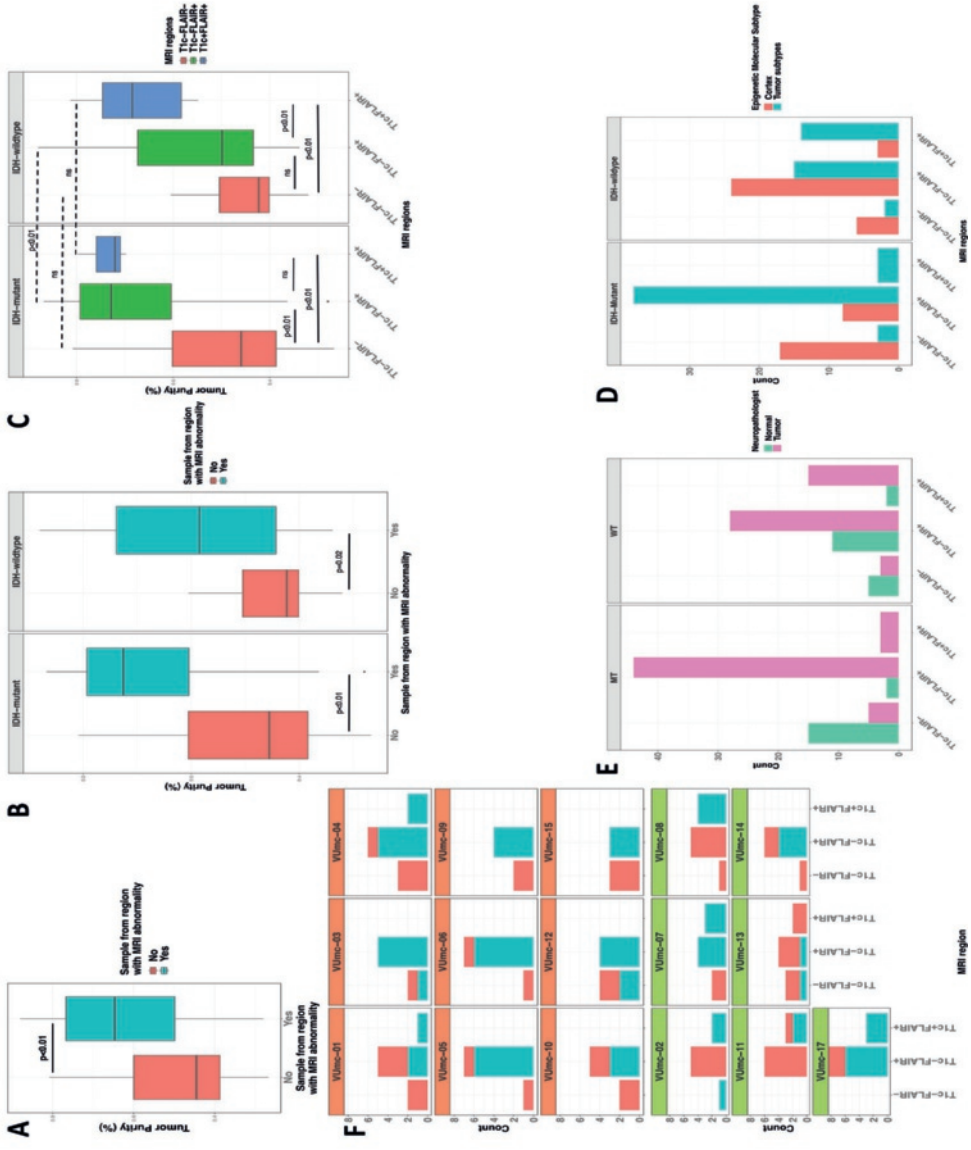
A
B
C
D
E
F
Tumor Purity (%)
Sample from region with MRI abnormality
No
Yes
p<0.01
p<0.02
ns
IDH-mutant
IDH-wildtype
MRI regions
T1c−FLAIR−
T1c−FLAIR+
T1c+FLAIR+
Epigenetic Molecular Subtype
Cortex
Tumor subtypes
Neuropathologist
Normal
Tumor
MT
WT
Count
MRI region
VUmc−01
VUmc−02
VUmc−03
VUmc−04
VUmc−05
VUmc−06
VUmc−07
VUmc−08
VUmc−09
VUmc−10
VUmc−11
VUmc−12
VUmc−13
VUmc−14
VUmc−15
VUmc−17

Figure 5 | Spatial distribution assessed with MRI regions (*page 202*).

A) Box plot of tumor purity for samples from regions with or without imaging abnormalities. B) Box plot of tumor purity for samples from regions with or without imaging abnormalities from IDH-mutant and IDH-wildtype gliomas. C) Boxplot of tumor purity of different MRI regions of IDH-mutant and IDH-wildtype gliomas. D) Bar plot of histopathological assessment of samples for each MRI region of IDH-mutant and IDH-wildtype gliomas. E) Bar plot of epigenetic molecular tumor subtypes and Cortex subtype of each MRI region of IDH-mutant and IDH-wildtype gliomas. F) Bar plot of epigenetic molecular tumor and Cortex subtypes for each MRI region for each patient, with label color according to IDH status.

Since MRI regions and DTTS where strongly correlated, we explored this correlation. This demonstrated a clear difference in the DTTS of the T1c-FLAIR- and T1c-FLAIR+ regions between IDH-mutant and IDH-wildtype gliomas (Supplementary Figure 3A). This is explained by the method of DTTS measurement that is based on distance to the FLAIR abnormalities in non-enhancing and to the T1c abnormalities in enhancing gliomas. Since the majority of IDH-mutant gliomas were non-enhancing (Supplementary Figure 3B), DTTS in the T1c-FLAIR+ regions was lower in IDH-mutant gliomas than in IDH-wildtype gliomas ($p<0.01$), which were more often enhancing (Fisher's exact $p<0.01$). The higher DTTS of IDH-wildtype gliomas in the T1c-FLAIR- region is because these samples were taken outside both the T1c and FLAIR abnormalities, while IDH-mutant samples from the same region were taken outside FLAIR abnormalities and therefore closer to the tumor surface. These findings illustrate the difference between MRI regions and DTTS for the different IDH status in gliomas and underline the necessity to further examine the spatial distribution of IDH-mutant and IDH-wildtype gliomas using DTTS. When comparing tumor purity with DTTS, both IDH-mutant and IDH-wildtype gliomas showed a significant negative correlation (Figure 6A). Using Fisher's z transformation, these correlations were comparable ($p=0.18$). This finding suggests a similar spatial distribution of IDH-mutant and IDH-wildtypes gliomas. However, results of the correlation between tumor presence by epigenetic molecular tumor subtypes and neuropathological assessment showed otherwise. DTTS of samples with an epigenetic molecular tumor subtype was higher in IDH-wildtype than in IDH-mutant gliomas ($p<0.01$) (Figure 6B). Also, the normalized DTSS, using the maximum core radius, was still higher in IDH-wildtype gliomas. This was similar for samples assessed as tumor by the neuropathologist (Figure 6B). One could argue that this was influenced by the size of the imaging abnormalities. However, there was no difference in maximum core radius between IDH-mutant and IDH-wildtype gliomas

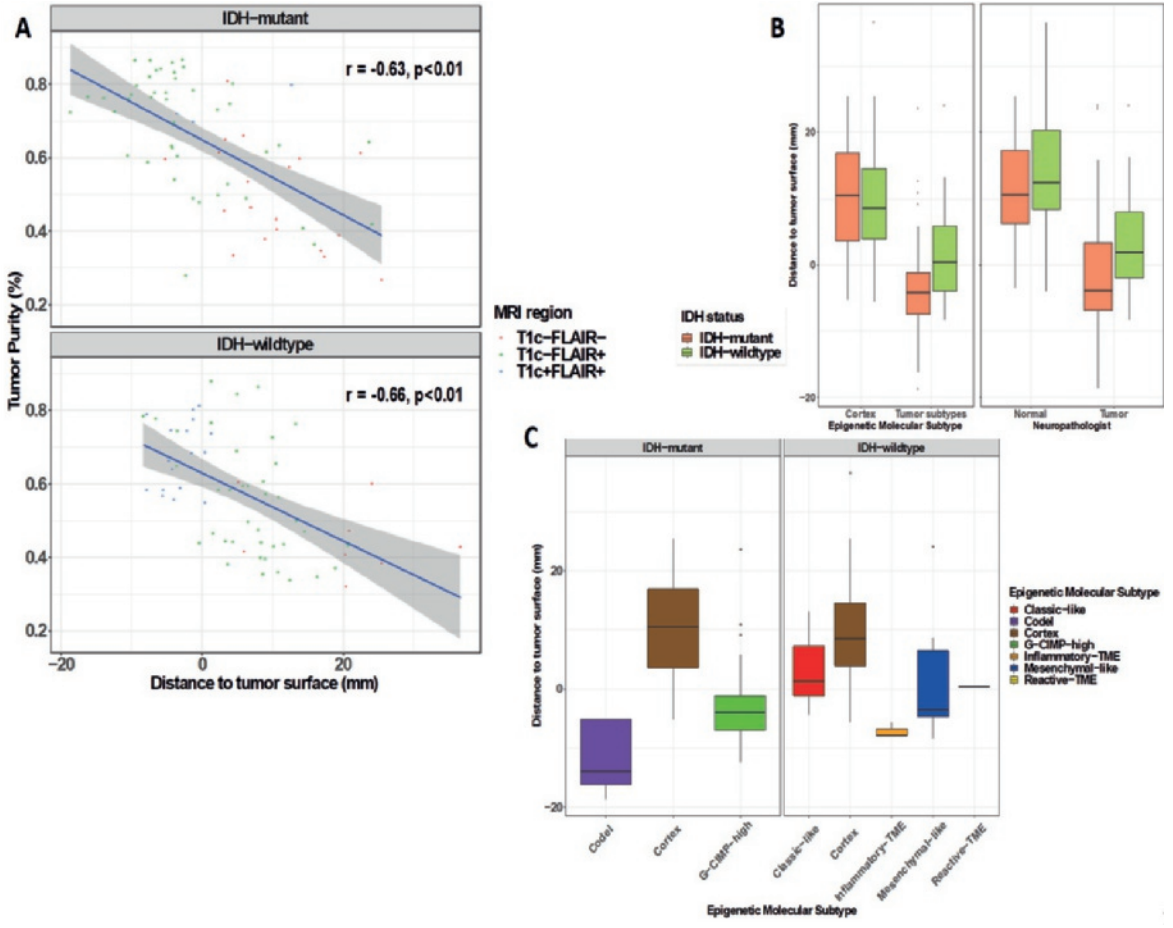

Figure 6 | Spatial distribution assessed with distance to tumor surface.
A) Correlation of tumor purity and distance to tumor surface of IDH-mutant (*top*) and IDH-wildtype (*bottom*) gliomas with the Pearson correlation coefficient. Colors represent the MRI regions of the samples. B) Boxplot of DTTS of epigenetic molecular tumor and Cortex subtypes (*left*) and histopathological assessment of tumor presence (*right*) of IDH-mutant and IDH-wildtype gliomas. F) Boxplot of DTTS of epigenetic molecular subtypes of IDH-mutant and IDH-wildtype gliomas.

(Supplementary Figure 3C). We further analyzed the DTTS for the different epigenetic molecular subtypes. Interestingly, median DTTS of the Classic subtype was higher than the median DTTS of both the Codel and the G-CIMP-high subtypes ($p<0.01$ for both), however, median DTTS of the Mesenchymal subtype was not ($p=0.14$ and $p=0.38$, respectively) (Figure 6C).

Overall, our findings imply that IDH-wildtype gliomas are more widespread beyond the standard MRI abnormalities than IDH-mutant gliomas and demonstrate the limitations of T1c MRI guided resections in IDH-wildtype gliomas.

Tumor purity largely explains spatial heterogeneity of epigenetic molecular subtypes

To explore the spatial distribution of epigenetic molecular subtypes, we compared the epigenetic molecular subtypes within each patient. Spatial heterogeneity of epigenetic molecular subtypes was present in every patient (Figure 7A), however, in 24 of 27 patients this was solely due to the co-existence of epigenetic molecular tumor and non-tumor subtypes. In three patients, more than one epigenetic molecular tumor subtype was identified (Figure 7B). In patient VUmc-05, five samples were classified as Codel with tumor purities ranging from 72% to 78%, while the one sample classified as G-CIMP-high showed a tumor purity of 61%. In patient VUmc-17, seven samples were classified as Classical (tumor purity 76–88%) and one sample was classified as Mesenchymal (tumor purity 61%). Finally, in patient Toronto-02, three samples were classified as Mesenchymal (tumor purity 86–89%) and two samples as Classical (tumor purity 76% and 82%). These results identify tumor purity as driving factor of spatial subtype heterogeneity, implying that (quantity and quality of) the admixture of non-neoplastic cells is the cause of a different epigenetic molecular subtype rather than clonal evolution.

To confirm the influence of tumor purity on the epigenetic molecular subtype classification, we compared the simplicity score of patients with and without epigenetic molecular tumor subtype heterogeneity since we already demonstrated that simplicity score and tumor purity were correlated. As expected, the median simplicity score was lower in patients with epigenetic molecular tumor subtype heterogeneity than without epigenetic molecular tumor subtype heterogeneity (61% versus 96%, $p=0.036$, Figure 7C), indicating that a lower classification probability is more likely to result in epigenetic molecular subtype heterogeneity. To further explore the influence of tumor purity on epigenetic molecular subtypes we plotted all samples, including the non-neoplastic

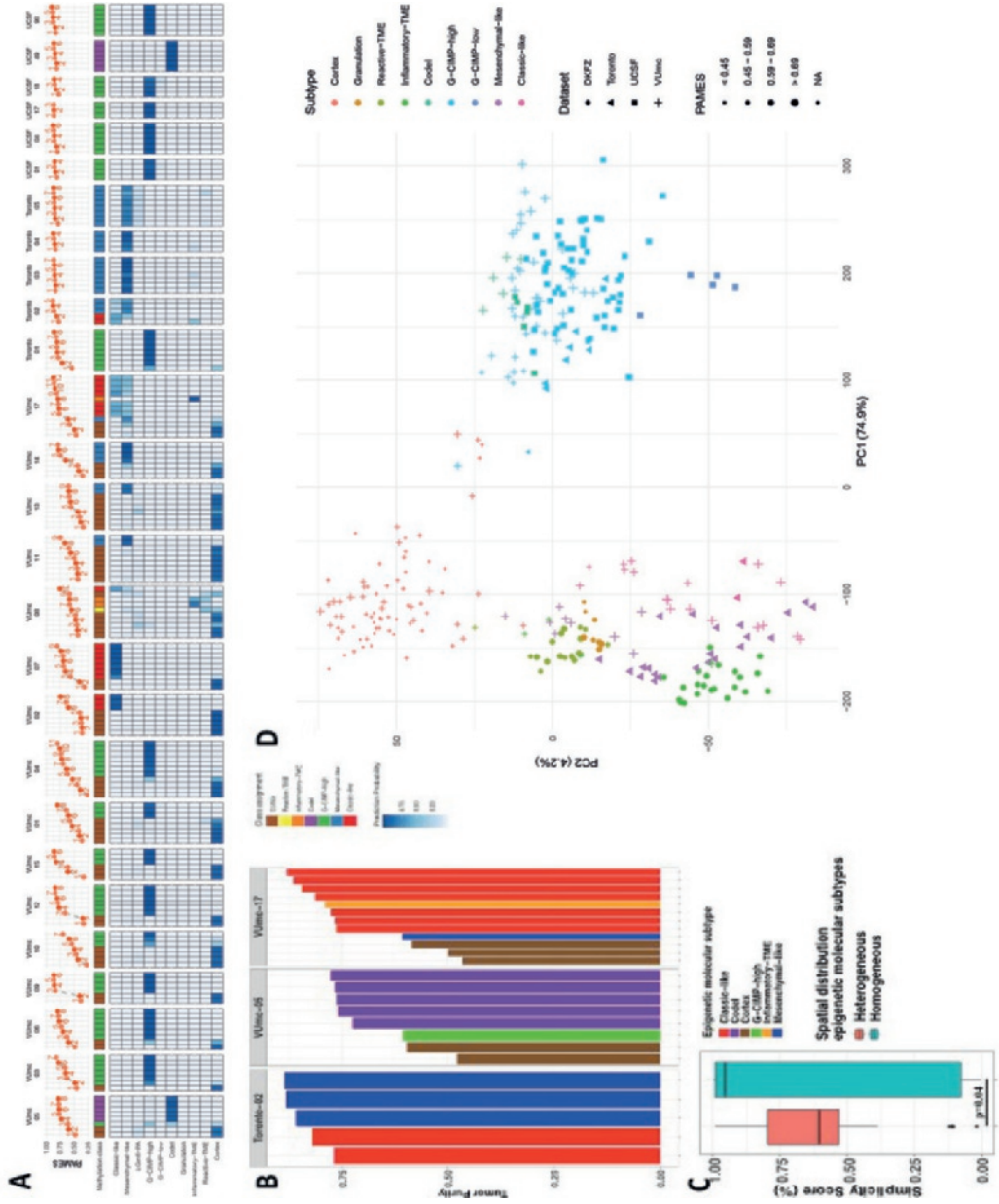
A
RMES
B
Tumor Purity
C
Spatial distribution epigenetic molecular subtypes
Heterogeneous
Homogeneous
Epigenetic molecular subtype
Classic-like
Codel
Cortex
G-CIMP-high
Inflammatory-TME
Mesenchymal-like
Stripeicity Score (%)
D
Subtype
Cortex
Granulation
Reactive-TME
Inflammatory-TME
Codel
G-CIMP-high
G-CIMP-low
Mesenchymal-like
Classic-like
Dataset
DKFZ
Toronto
UCSF
VUmc
RMES
< 0.45
0.45 – 0.59
0.59 – 0.69
> 0.69
NA
PC1 (74.9%)
PC2 (4.2%)

Figure 7 | Spatial heterogeneity of DNA methylation classification (*page 206*).

A) Overview of DNA methylation classification with classification probability for exploration and validation cohort. B) Bar plot of tumor purity and epigenetic molecular subtype of three patients with spatial heterogeneity. C) Boxplot of simplicity score for patients with and without spatial heterogeneity of epigenetic molecular subtypes. D) Principal component analysis of both exploration, validation and normal samples.

cohort, with a principal component analysis (PCA) (Figure 7D). Two distinct patterns were identified in this PCA. First, samples were separated left to right by their IDH mutational status, with IDH-wildtype samples on the left and IDH-mutant samples on the right. Second, samples were spread top to bottom by their tumor purity, with low purity in the top and high purity in the bottom.

These findings indicate that tumor purity accounts for a considerable amount of variation in the data and affirms the influence of tumor purity on spatial heterogeneity of epigenetic molecular subtypes.

Spatial heterogeneity of genome-wide methylomes is innate and not a feature of glioma
Tumor heterogeneity is considered a salient feature of gliomas and thought to be a driver of treatment resistance and disease progression. Extensive multi-sector samples with at least six samples per patient in this study provide a unique opportunity to carefully define and quantify spatial heterogeneity in DNA methylation.

To precisely quantify DNA methylation heterogeneity, we performed pairwise comparisons of binarized methylation values using all possible combinations of any two samples of all cohorts, providing percentages of heterogeneous probes between any two samples. The vast majority of probes were homogeneously methylated (mean 0.93, range 0.83–1.0), suggesting that only a small fraction of probes is responsible for all tumor heterogeneity. Hierarchical clustering of both exploration and validation cohort using these heterogeneity values as a distance metric separated samples by IDH status and tumor/normal classification first and patient second, suggesting that distinctly classified samples within a patient should be analyzed separately (Figure 8A).

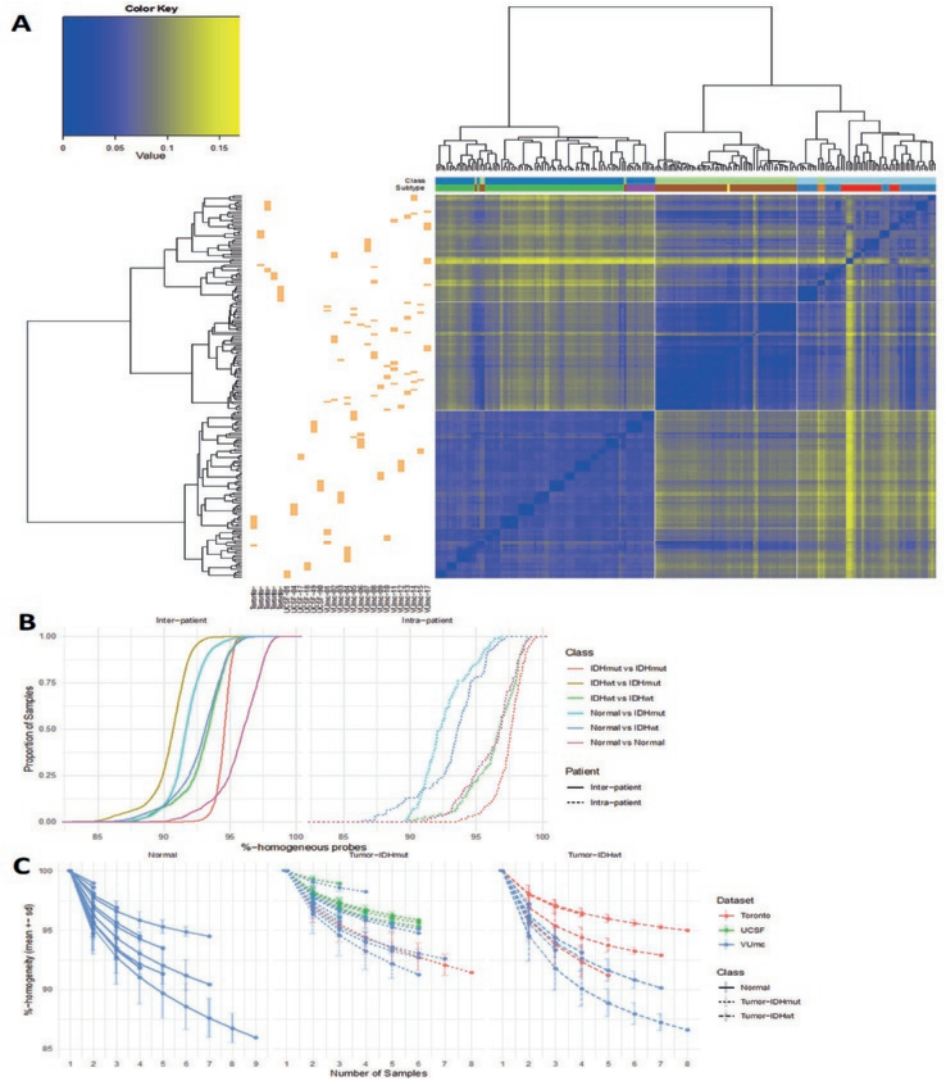

Figure 8 | Spatial heterogeneity of genome-wide methylomes.

A) Hierarchical clustering of intratumorale heterogeneity B) Empirical cumulative density function (ECDF) curves reflecting similarity (homogeneity) across all pairwise combinations of samples. Comparisons were separated based on whether they involved two samples from the same patient (intra-patient) or between two patients (interpatient) and based on whether the two samples spanned one or multiple sample types. C) Line plot showing the cumulative homogeneity associated with additional samples taken from the same tumor. Lines were colored by dataset, tumor and normal samples were separated, and tumor samples were further separated into IDHmut and IDHwt.

Unsurprisingly, any two samples from different tumors showed less probes with similar methylation (mean 0.93 ± 0.02) compared to any two samples from the same tumor (mean 0.96 ± 0.03), although this difference was subgroup-dependent. For example, any two samples from two distinct IDH-mutant tumors show much more similarity on average than any two samples from two distinct IDH-wildtype tumors (Figure 8B), likely related to the propensity of IDH-mutant tumors to uniformly methylate. As expected, a large degree of heterogeneity can be observed when comparing samples classified as normal to samples classified as tumor, based on DNA methylation classification, within the same patient (note: light blue and blue dashed lines).

Any two IDH-wildtype tumor samples from the same patient show a comparable degree of heterogeneity as any two normal samples from the same patient (P=1.0, pink and green dashed lines). More strikingly, any two IDH-mutant tumor samples from the same patient demonstrate less heterogeneity compared to any two normal samples from the same patient (P<0.0001). These findings suggest that heterogeneity in DNA methylation is innate to the individual and is not a feature of diffuse glioma. In fact, IDH-mutant tumors lose the innate heterogeneity that is present between normal cells and can be characterized by a loss of heterogeneity.

To assess the impact of additional samples on tumor heterogeneity we calculated the percentage of identical probes pooling any number of samples per patient, separating samples classified as tumor and normal (Figure 8C). The majority of heterogeneity was captured by the first two samples per patient. Although additional samples further contributed to overall heterogeneity, the change heterogeneity decreased exponentially with each additional sample. The decline in heterogeneity with each additional sample showed comparable patterns in normal and tumor sets of samples, further underlining the notion that heterogeneity in DNA methylation is largely determined by innate tissue (rather than tumor cell) characteristics.

DISCUSSION

This study represents a multimodality analysis of core and peripheral samples in diffuse glioma. The combination of histological, radiological and DNA-methylation data enabled to explore tumor purity, spatial distribution of epigenetic molecular subtypes and spatial genome-wide DNA methylation heterogeneity. Our main finding is the intratumoral

stability of epigenetic molecular subtypes after considering purity, which was validated in an external cohort. Furthermore, genome-wide DNA methylation heterogeneity was found to be larger than epigenetic molecular subtype heterogeneity, however, still considerably less than reported mutational and transcriptional heterogeneity. Also, we found the DNA-methylation derived tumor purity estimate reflects tumor purity best and that the spatial distribution of this estimate shows a more extensive diffuse infiltrative growth at the time of first surgical intervention in IDH-wildtype than IDH-mutant diffuse gliomas.

Information on spatial heterogeneity of epigenetic molecular subtypes in the literature is limited. A recent study with 38 multi-sector samples reported epigenetic molecular subtype heterogeneity in 5 of the 12 patients with a glioblastoma based,[339] consisting of both Mesenchymal and RTKI or RTKI and RTKII classes, according to Capper et al.[342] Interestingly, they also concluded that spatial heterogeneity was caused by tumor purity, rather than tumor evolution, in the majority of heterogeneous patients. Besides tumor purity, the difference in classification method could explain their higher percentage of spatial heterogeneity, since the RTK I class from Capper et al. does not have a direct representation in the Ceccarelli et al. classification.[341,342] We also found samples outside imaging abnormalities on FLAIR in non-enhancing and on T1c MRI in enhancing gliomas to display similar epigenetic molecular subtypes as the core samples. Interestingly, tumor purity differed between the different MRI regions. These findings suggest that spatial imaging heterogeneity in glioma is driven by tumor purity, rather than epigenetic heterogeneity. It further implies that a viable part of the tumor, especially in IDH-wildtype gliomas, is left behind after resection of standard imaging abnormalities.

Tumor heterogeneity has long been viewed as a hallmark of cancer and the idea that various tumorigenic clones compete for resources and evolve in response to treatment pressure is widely accepted. Nevertheless, it is easy to overestimate the role and importance of epigenetic tumor heterogeneity and a more nuanced role for heterogeneity is slowly gaining traction.[349] Our analysis shows no clear differences in degree/level of DNA methylation heterogeneity in tumor tissue compared to non-neoplastic brain tissue, suggesting that in this context a substantial part of the heterogeneity that is detected by DNA methylation is innate rather than tumor-driven. In fact, we demonstrated that DNA methylation heterogeneity in IDH-mutant diffuse gliomas is less heterogeneous compared to surrounding non-neoplastic brain tissue. Large multi-time point studies

of pre- and post-treatment diffuse gliomas are needed to better understand how heterogeneity responds to treatment and how it changes over time.

Tumor purity estimates differ between measurement modalities, with the DNA methylation based PAMES metric as most representative. Since clinical practice demands for tumor purity estimation before acquisition of tissue radiologic assessment of purity is indispensable. We found the imaging score, which is based on standard MRI abnormalities, to correlate well with PAMES and therefore useful for non-invasive purity assessment. Multimodality advanced imaging has recently been reported as good predictor of proliferation index.[350] However, proliferation index was least correlated with PAMES in our study and therefore not the most promising modality for assessment of tumor purity. Therefore, studies predicting tumor purity with multimodal imaging are needed. Furthermore, our data shows a difference in glioma infiltration patterns between IDH-mutant and IDH-wildtype diffuse gliomas. IDH-wildtype gliomas demonstrate a more gradual decline in glioma infiltration, whereas. IDH-mutant gliomas reveal a more binary distribution, indicating a somewhat less extensive diffuse infiltrative growth. Finally, we found discordance between histopathological assessment and epigenetic molecular classification specially is samples assessed as tumor by the neuropathologists. These findings could reflect the difficulty of identification of tumor cells among non-neoplastic altered normal brain by the neuropathologist, or, other way around, the lower sensitivity of the DNA methylation-based tumor purity metric for very low tumor content.

METHODS

Sample acquisition

The exploration cohort consisted of 16 patients with an untreated initial diffuse glioma, treated at the Amsterdam UMC, location VU medical center (VUmc), Amsterdam, The Netherlands. Multi-sector sampling was performed, using a stereotactic biopsy procedure preceding the craniotomy, to obtain two samples of each biopsy location for, respectively, FFPE and *Molfix*© *(*patient 1–8*)* or snap-frozen (patient 9–16) fixation. The protocol of this study has been published,[201] was approved by the Medical Ethics Committee of the VUmc and registered in the Dutch National Trial Register (www.trialregister.nl, unique identifier NTR5354). All procedures were carried out in accordance with the Helsinki Declaration.[351] Written informed consent was obtained from all patients.

The validation cohort comprised 11 patients with 61 FFPE samples from multi-sector sampling of an untreated diffuse glioma treated at the Toronto Western Hospital, Toronto, Canada or USCF Brain Tumor Center, San Francisco, USA. In addition, 64 FFPE samples from 64 patients without a glioma from the German Cancer Network served as controls.

DNA isolation

DNA isolation was performed by adding proteinase K and incubation at 56°C using QIAamp DNA Mini Kit (Qiagen). DNA was quantified using a Qubit Fluorometer (ThermoFisher). Genomic DNA was bisulfite converted using Qiaamp DNA FFPE tissue Kit (Qiagen).

DNA methylation profiling by microarray

Data was processed using the minfi packages in R (R Foundation for Statistical Computing, Vienna). Data from the 450k (IlluminaHumanMethylation450k.ilmn12.hg19) and EPIC platforms (IlluminaHumanMethylationEPICanno.ilm10b2.hg19) were processed separately. Detection P-values were calculated for each probe and sample, and samples with an average detection P-value >0.01 were removed from follow-up analysis. Data was normalized using BMIQ from the wateRmelon package in R. Probes on sex chromosomes and known cross-reactive probes were removed, as were probes mapping to known SNPs and probes with a detection P-value >0.01. Finally, data from different platforms was merged.

DNA-methylation based classification and simplicity score

Glioma methylation subtype classification was performed using L2-regularized logistic regression using the R package LiblineaR. Classifiers were trained and evaluated on a set of common probes from TCGA glioma samples with known methylation subtypes. The classes LGm6-GBM and PA-like were merged into a single class LGm6-PA as the separation between these classes was based on phenotype. To improve classification accuracy of samples with low tumor purity, DKFZ controls were added to the classifier as separate classes.

Methylation purity estimation and simplicity score

DNA methylation measurements of tumor purity included the PAMES algorithm and simplicity score.[344,345] For the PAMES normal central nervous system samples from the German Cancer Research Center (DKFZ) were used as a control. PAMES operates in three steps. First, AUCs are calculated for each probe discriminating between tumor and

normal. Second, a selection of the most informative probes is made. Third, tumor purity is calculated on input samples using these probes

DNA copy number aberrations inferred from EPIC microarray

Using the R/Conumee package, copy number aberrations were inferred from the 450k and EPIC array data. Merged data from the control samples was used as baseline control for all analyses. Genomic data was used to calculate aneuploidy.

Immunohistochemistry and qualitative assessment

FFPE samples from the exploration cohort were stained using hematoxylin and eosin (HE) and MIB-1. Two expert neuropathologists independently, blinded for imaging results, assessed the presence or absence of tumor in each sample. Consensus was obtained in case of disagreement. The patient's histopathological diagnosis was made based on resection material using routine procedures and according to the WHO 2016 criteria.[9]

Histopathological analysis of whole-slide scans

Using a Hamamatsu Nanozoomer XR, FFPE slides stained with HE and MIB-1 of each sample were digitalized. The 40x magnification images were converted to multiple mosaic images using NDPITools software. Cellularity, defined as number of cells per mm^2, was calculated with Cellprofiler. Proliferation index, defined as percentage of Ki-67 positive nuclei of all nuclei, was calculated using local developed software.

Radiologic evaluation of sample locations

Standard imaging sequences from the patients in the exploration cohort included T1-, T2-, T2/FLAIR and T1c MRI. For each sample location presence of an abnormal signal for each imaging sequence was independently assessed by a neurosurgeon and neurosurgical resident with ample experience in glioma imaging. Consensus was obtained in case of disagreement.

Sample-to-tumor surface distance

Tumors were segmented on FLAIR and T1c MRI, using Brainlab Software, by a neurosurgical resident with ample experience in glioma imaging. The segmentations and sample coordinates were exported in 3D T1c MRI space and sample to tumor-surface distances were calculated using Matlab.

Statistical analysis

Median values with interquartile range (IQR) were used to describe non-normally distribute data. Mann-Whitney-U test was used to compare distributions between subgroups. Correlations were calculated with the Spearman or Pearson's correlation and compared using Fisher's z transformation. Comparison of percentages between subgroups was performed using Fisher's test Normalization and scaling of purity measurement modalities was performed by subtracting the mean and dividing by the SD. To compare absolute purity estimates, the normalized and scaled purity measurements were rescaled using the PAMES mean and SD. P values less than 0.05 was considered statistically significant. R (version 3.5.3) was used for all statistical analyses.

Heterogeneity analysis

Each probe per patient was classified as methylated (B>=0.3) or unmethylated (B<0.3). A table of all possible pairwise combinations of samples was generated. Each pair of samples was evaluated for heterogeneity by counting the number of identical (homogeneous) probes, the number of differing (heterogeneous) probes and percentages were subsequently calculated. Each pair was annotated according to the metadata for each sample in the comparison.

For each patient and sample type we tabulated all possible combinations of any number samples, iteratively including between 1 and the total number of possible samples. The proportion of heterogeneous and homogeneous probes was calculated when considering each sample in a given set. For each patient/sample type and sample number we then calculated the mean and standard deviation of the proportion heterogeneous across all sets.

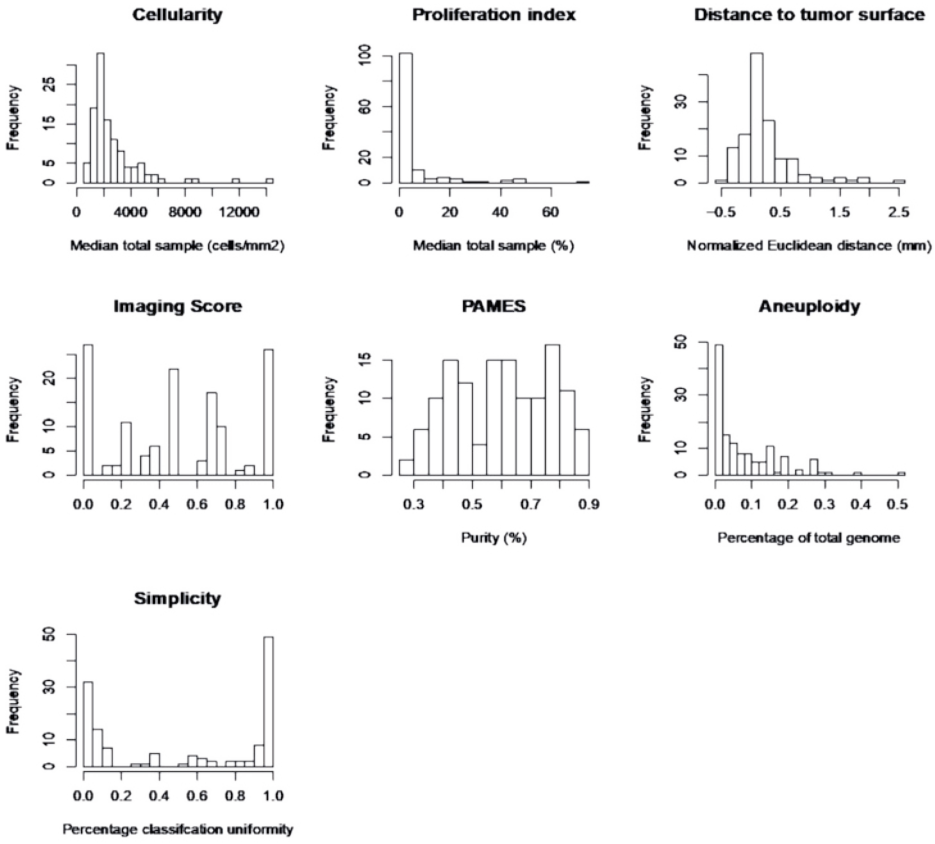

Supplemental Figure 1 | Distribution of individual tumor purity measurement modalities

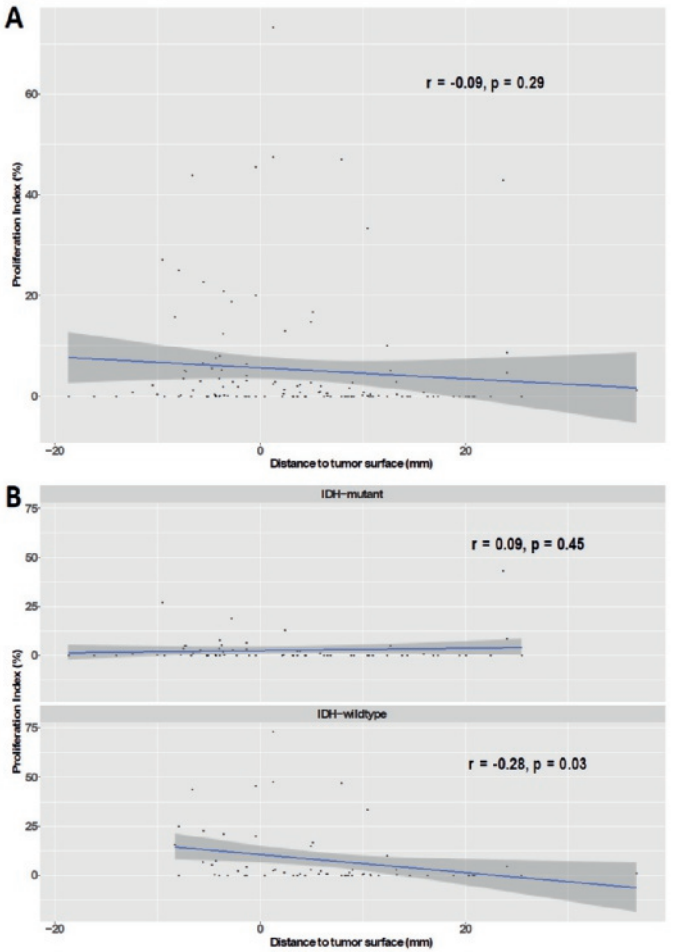

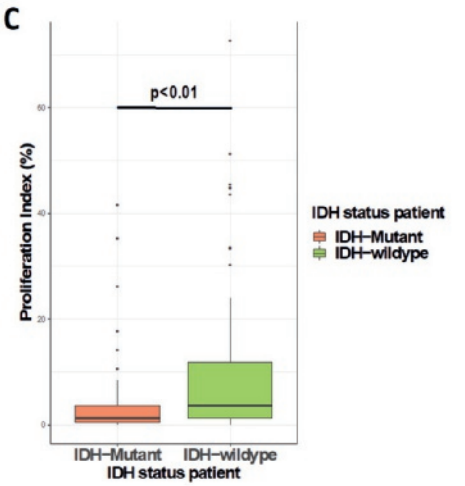

Supplemental Figure 2 | Exploration of abscence of correlation between distance and proliferation index.

A) Scatterplot of DTTS and proliferation index of all samples with Pearson's correlation coefficient. B) Scatterplot of DTTS and proliferation index of samples from IDH-mutant and -wildtype gliomas with Pearson's correlation coefficient C) Boxplot of proliferation index of samples from IDH-mutant and -wildtype gliomas demonstrating the lower proliferation index in IDH-mutant gliomas.

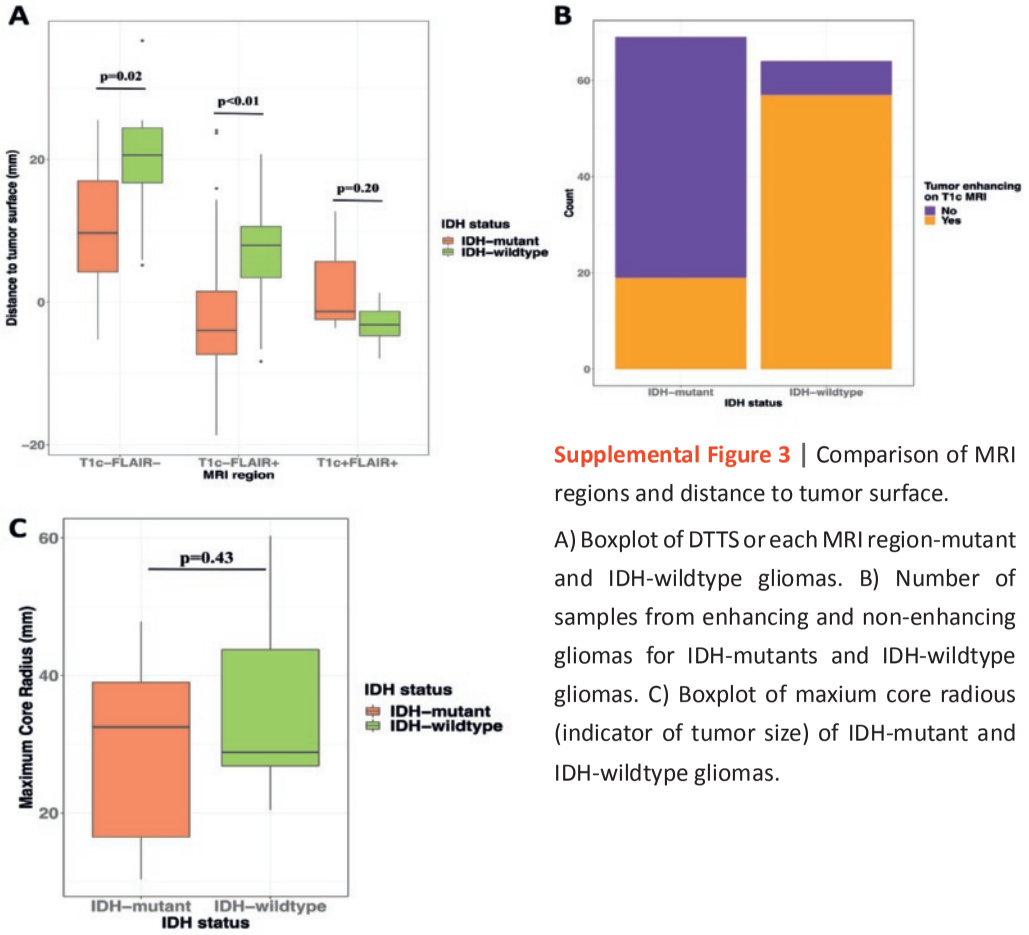

Supplemental Figure 3 | Comparison of MRI regions and distance to tumor surface.

A) Boxplot of DTTS or each MRI region-mutant and IDH-wildtype gliomas. B) Number of samples from enhancing and non-enhancing gliomas for IDH-mutants and IDH-wildtype gliomas. C) Boxplot of maxium core radious (indicator of tumor size) of IDH-mutant and IDH-wildtype gliomas.